Molecular dynamics simulation of a nanoscopic nematic twist cell

Leonid V. Mirantsev
Institute for Problems of Mechanical Engineering, Russian Academy of Sciences, 199178, St. Petersburg, Russia

Epifanio G. Virga
Dipartimento di Matematica and CNISM, Università di Pavia, via Ferrata 1, 27100 Pavia, Italy

(Received 4 May 2007; published 15 August 2007)

We present molecular dynamics simulations of a nanoscopic nematic twist cell confined within two bounding substrates with conflicting anchoring conditions. The results of our simulations show that the torque transmitted through the cell drops significantly below a certain critical cell's thickness, thus confirming the predictions of the continuum Landau theory extrapolated down to the nanoscopic scale [F. Bisi, E. G. Virga, and G. E. Durand, Phys. Rev. E **70**, 042701 (2004)].

DOI: 10.1103/PhysRevE.76.021703 PACS number(s): 61.30.Cz, 61.30.Dk, 61.30.Pq

I. INTRODUCTION

In the last few years, certain structural transitions in nematic liquid crystals confined within electro-optical cells have been interpreted in a different, innovative manner. Starting from the work of Martinot-Lagarde *et al.* [1], which interpreted earlier experiments [2], the hypothesis gradually emerged that molecular reorganizations under the effect of an electric field could result from an *order reconstruction*, a process that does not involve rotations of the nematic director $\boldsymbol{n}$, which represents the average molecular orientation, and yet connects two antagonistic uniaxial states through a range of states where the molecular distribution is no longer uniaxial and globally less ordered. The order tensor $\mathbf{Q}$ is traditionally employed [3] to describe these intermediate states. The tensor $\mathbf{Q}$ is symmetric and traceless; it describes uniaxial states when two of its eigenvalues coincide, and biaxial states when all of its eigenvalues are different from one another. An order reconstruction takes place whenever two conflicting uniaxial states, possibly prescribed by anchoring conditions on antagonistic bounding substrates, are reconciled in space through a variety of biaxial states, implying nearly no rotation in the eigenframe of $\mathbf{Q}$: one uniaxial state emerges, as it were, from another via the disruption of one alignment and the construction of another, through states with no single alignment.

Both theory and experiment [4–7] have attempted to retrace the signs of this mechanism, especially when alternative mechanisms could also explain the observed data. Such is, for example, the case of *anchoring breaking* [8], which postulates that the electro-optic transition between two topologically distinct textures in a π cell is achieved through a momentary failure of the anchoring to a substrate. Evidence has been collected that also supports the interpretation of this transition in terms of surface order reconstruction, a phenomenon taking place near an anchoring substrate so strong as to hold in place the nematic molecules stuck on it [9].

Order reconstruction, both in bulk and on anchoring substrates, occurs across an extended biaxial wall, similar in structure to the one wrapped around a disclination's core [10,11]. For example, in a $\frac{1}{2}$ disclination, orthogonal nematic alignments are reconciled through an *exchange* of eigenvalues [11] in the spectral representation of $\mathbf{Q}$, which is nothing but an order reconstruction confined within a line defect.

The link between order reconstruction and defects goes indeed beyond the analogy just recalled. It was recently shown [12] that in the presence of a disclination the electric field needed to produce the desired commutation between molecular textures in a hybrid nematic cell is considerably weaker than in the absence of disclinations; such a threshold reduction, also observed in experiments [4], results from the interaction between the biaxial wall associated with the order reconstruction and the biaxial ring concealed within the disclination's core [10]. A different mechanism [13], also assigning a role to defect motion, predicts a similar threshold reduction in a π cell.

All these phenomena are driven by electric fields with a coherence length comparable to the biaxial coherence length ξ_b [10], which is nanoscopic in size. In [14] we explored the possibility of inducing order reconstruction within a nematic twist cell by drawing the bounding plates down to separations comparable with ξ_b. We found that order reconstruction can indeed be detected mechanically [15,16], thus actually changing the cell into an ideal torque nanomachine: the signature of order reconstruction would be a *snapping* instability of the machine, heralded by the lack of monotonicity in the torque diagram against the cell's thickness. Such an instability might have already been observed, albeit in a different geometric setting [17]. A similar instability was also predicted for the interaction between two parallel nanocylinders enforcing the homeotropic anchoring on the nematic liquid crystal surrounding them [18].

These conclusions were drawn by extrapolating the continuum Landau theory of liquid crystals down to the nanoscopic scale, an approach which may well be regarded as extreme. To explore the validity of this extrapolation, we devote this paper to a molecular dynamics study that has nothing in common with our previous studies [14–16], except for the geometric setting and the anchoring conditions of the equilibrium problem.

A vast literature already exists on confined nematic liquid crystals. Some studies employ computer molecular simulations [19–36], among which, in particular, several are performed on a lattice [25,26,31,33,34], as will be ours. Other studies employ density functional theory [37–43], and still

others combine this method and computer simulations [44–46] (the reader is referred to [35] for a broad perspective on the literature presented). However, to the best of our knowledge, the torque transmitted from one confining surface to another has not yet been addressed by any of these computational methods.

The paper is organized as follows. In Sec. II, we write the evolution equations solved in our molecular simulations. In Sec. III, we illustrate the simulation results, placing special emphasis on the torque transmitted from one anchoring plate to the other at equilibrium, the crucial property to explore being the monotonicity of the torque diagram. Finally, in Sec. IV we summarize our conclusions and assess the legitimacy of extrapolating the continuum Landau theory down to the nanoscopic scale.

II. EQUATIONS AND SIMULATION DETAILS

We consider a cell containing a nematic liquid crystal (LC) confined between two plane, parallel plates set at a nanoscopic distance d apart. Here we take a molecular view and regard this cell as an ensemble of elongated molecules modeled as unit spins with centers of mass fixed at the sites of a face-centered-cubic lattice. These spins, however, retain all orientational degrees of freedom. The rotation of the ith spin is governed by the following equations:

$$\dot{\boldsymbol{e}}_i = \boldsymbol{\omega}_i \times \boldsymbol{e}_i, \tag{1}$$

$$I\dot{\boldsymbol{\omega}}_i = \boldsymbol{\tau}_i. \tag{2}$$

Here, a spin is represented as a unit vector $\boldsymbol{e}_i$, and $\boldsymbol{\omega}_i$ is the corresponding angular velocity; $\boldsymbol{\tau}_i$ is the total torque exerted on the ith molecule from both the other LC molecules and the molecules in the anchoring substrates, and I is the molecular moment of inertia. Though nematic molecules are elongated, so as to make it plausible describing them as *nonpolar* spins, here, for simplicity, the molecular tensor of inertia is assumed to be isotropic, and thus characterized by a single moment of inertia I, which is further taken to be a unit in the scaled molecular dynamics (MD) units [47].

The plates bounding the cell promote specific orientations of the LC molecules lying in their vicinity. Such boundary conditions are modeled here by treating the molecules comprising the plates' anchoring substrates as fixed unit spins with prescribed orientations, which interact with the LC molecules in a considerably stronger manner than LC molecules do with one another. We take both bounding plates parallel to the (x,y) plane of a Cartesian coordinate frame (x,y,z). We assume that the molecules of one substrate are aligned along the x axis, whereas the molecules in the opposite substrate make the angle Φ_0 with the x axis.

Both the interaction between LC molecules and the interaction between these and the molecules in the two anchoring substrates are described by McMillan's anisotropic pair potential [48]. Precisely, the interaction energy between the ith and jth molecules is given in the form

$$V_{ij}^{(M)}(r_{ij},\vartheta_{ij}) = -V_{ij}P_2(\cos\vartheta_{ij})\exp(-r_{ij}^2/r_0^2), \tag{3}$$

where $P_2(u) := \frac{1}{2}(3u^2-1)$ is the second Legendre polynomial, r_{ij} is the distance between the centers of mass p_i and p_j of the two interacting molecules, ϑ_{ij} is the angle between their long axes, i.e., $\cos\vartheta_{ij} := \boldsymbol{e}_i\cdot\boldsymbol{e}_j$, $V_{ij}>0$ is the interaction strength, and r_0 is a characteristic length of this short-range interaction, which is of the order of the molecular size (~ 1 nm).

The total force $\boldsymbol{f}_i$ and the total torque $\boldsymbol{\tau}_i$ acting on the ith molecule are given by

$$\boldsymbol{f}_i = \sum_{j=1,j\neq i}^{N} \boldsymbol{f}_{ij} \quad \text{and} \quad \boldsymbol{\tau}_i = \sum_{j=1,j\neq i}^{N} \boldsymbol{\tau}_{ij}, \tag{4}$$

respectively, where N is a total number of molecules in the system and

$$\boldsymbol{f}_{ij} = -\left(\frac{\partial V_{ij}^{(M)}}{\partial r_{ij}}\right)\boldsymbol{e}_{ij} \quad \text{with} \quad \boldsymbol{e}_{ij} := \frac{\boldsymbol{r}_{ij}}{r_{ij}}, \tag{5}$$

$$\boldsymbol{\tau}_{ij} = -\left(\frac{\partial V_{ij}^{(M)}}{\partial \cos\vartheta_{ij}}\right)\boldsymbol{e}_i \times \boldsymbol{e}_j. \tag{6}$$

Here, $\boldsymbol{r}_{ij} := p_i - p_j$ is the vector drawn from the center of mass p_j of the jth molecule to the center of mass p_i of the ith molecule. V_{ij} is taken to be a unit (in MD units) for interactions between LC molecules, while it is taken to be 10 times larger for interactions between LC molecules and the molecules in both anchoring substrates ($V_{\text{LC-SB}}/V_{\text{LC-LC}}=10$). Thus, we consider a *strong* anchoring between the nanoscopic LC cell and its bounding substrates.

The LC cell is resolved in a number of plane layers, each consisting of an (x,y) cut of the face-centered-cubic lattice, bearing $2\times 13^2=338$ molecular sites. The number of these layers varies from 20 down to 2, according to the different values of the cell's thickness explored here. Thus, the total number of molecules in the confined cell ranges from 676 to 6760, while correspondingly the number of molecules in each solid substrate ranges from 4056 (12 layers) to 1014 molecules (three layers). The total number of molecules in the system is constant, and equal to 8778. More specifically, in our MD simulations, we increase the number of layers constituting the bounding substrates, while simultaneously decreasing the number of confined LC molecules, so that both the total number of layers and the total number of particles in the simulation box are conserved. Moreover, since McMillan's model potential is strongly short ranged, these changes in thicknesses in both the confined LC cell and the bounding substrates do not produce any appreciable change in the substrate-LC interaction: only three nearest layers for each substrate give a significant contribution to this interaction. Thus, in each case the LC cell is effectively bounded by very thin substrates. There are always 26 layers in our sample, and this is enclosed in a cubic simulation box $22r_0\times 22r_0\times 22r_0$ in size, where the characteristic length r_0 is taken to be 1 (in MD units). The apparent mismatch between the simulation box size and the number of layers is caused by our use of a face-centered-cubic lattice. The code creating

the simulation sample works as follows: We first set the number density of spins (1, in the present case) and the size of the simulation box ($22r_0 \times 22r_0 \times 22r_0$). Then the code determines both the number of spins and the lattice constant matching both these parameters, so that the lattice constant can differ from the length unit r_0, as it does here.

MD simulations are performed under periodic boundary conditions along both x and y axes, and at constant volume and constant reduced temperature $T^*:=k_BT/V_{\text{LC-LC}}$, where T is the temperature of the system, and k_B is the Boltzmann constant. In our model the nematic-to-isotropic transition takes place at $T^*_{\text{NI}}=0.61$. To determine this bulk transition temperature, we performed MD simulations on a similar system without substrates, composed of freely rotating spins under periodic boundary conditions along the x, y, and z axes. We started from a perfectly ordered state (all spins were oriented along the z axis) and followed the time evolution of the Maier and Saupe [49] orientational order parameter S averaged over all molecules of the system. It was found that, for $T^*>0.61$, S decays gradually to nearly zero, whereas, for $T^*\leq 0.61$, it reaches a certain nonzero value (for $T^*=0.61$, this value is equal to $S_{\text{NI}}\approx 0.4$). Thus, the reduced temperature $T^*_{\text{NI}}=0.61$ was taken as the bulk nematic-to-isotropic transition temperature. Since we were interested in the behavior of the system in the nematic phase, in all our simulations T^* was either 0.5, 0.55, or 0.58.

A single simulation is started either from a random orientation of the spins in the cell or from a linearly twisted configuration. All simulations are run for 200 000 time steps (one time step is equal to 0.001 in dimensionless MD units) until an equilibrium state of the system is reached. At each time step, Eqs. (1) and (2) are solved numerically by using the algorithm described in [47] (see, in particular, Chap. 3), and the temperature of the system is kept constant by appropriately rescaling the angular velocities.

To describe the orientational order of the molecules in the cell, we define for the kth layer the orientational order parameter S_k, the average nematic director $\boldsymbol{n}_k$, and the biaxiality parameter b_k, to be computed at all steps of the simulation process. As in [47,50,51], these observables are derived from the symmetric, traceless order tensor $\mathbf{Q}_k$ defined for the kth layer as

$$\mathbf{Q}_k := \frac{3}{2N_k}\sum_{i=1}^{N_k} \boldsymbol{e}_i \otimes \boldsymbol{e}_i - \frac{1}{2}\mathbf{I}, \tag{7}$$

where the sum is extended over the N_k molecules in the kth layer, and $\mathbf{I}$ is the identity tensor. The orientational order parameter S_k is identified with the largest eigenvalue $\lambda_k^{(1)}$ of $\mathbf{Q}_k$, while the average nematic director $\boldsymbol{n}_k$ is in turn identified with the eigenvector of $\mathbf{Q}_k$ corresponding to $\lambda_k^{(1)}$. The biaxiality parameter b_k is then defined as

$$b_k := \frac{1}{3}(\lambda_k^{(2)} - \lambda_k^{(3)}), \tag{8}$$

where $\lambda_k^{(2)}$ and $\lambda_k^{(3)} \leq \lambda_k^{(2)}$ are the eigenvalues of $\mathbf{Q}_k$ other than $\lambda_k^{(1)} > \lambda_k^{(2)}$. For each layer, $\boldsymbol{n}_k$ can be represented in terms of a polar angle θ_k and an azimuthal angle ϕ_k by the following formula:

$$\boldsymbol{n}_k = (\sin\,\theta_k \cos\,\phi_k)\boldsymbol{e}_x + (\sin\,\theta_k \sin\,\phi_k)\boldsymbol{e}_y + (\cos\,\theta_k)\boldsymbol{e}_z, \tag{9}$$

where $(\boldsymbol{e}_x, \boldsymbol{e}_y, \boldsymbol{e}_z)$ is the frame of unit vectors associated with the Cartesian coordinates (x, y, z).

The univocal definition of $\boldsymbol{n}_k$ properly relies on the existence of a single maximum eigenvalue of $\mathbf{Q}_k$: if $\lambda_k^{(1)}=\lambda_k^{(2)} \geq \lambda_k^{(3)}$ then $\boldsymbol{n}_k$ would be any unit vector in the plane orthogonal to the eigenvector of $\mathbf{Q}_k$ associated with $\lambda_k^{(3)}$, this implying a similar degeneracy in the representation formula (9). A state where the two largest eigenvalues of $\mathbf{Q}_k$ coincide is often called *planar uniaxial*. We adopt here this terminology and hold that for a planar uniaxial state $\boldsymbol{n}_k$ degenerates in the whole unit circle $\mathbb{S}^1$, whereas S_k remains well defined. The occurrence of a planar uniaxial state is also reflected in the representation of $\boldsymbol{n}_k$ in Eq. (9): there both θ_k and ϕ_k may suffer a discontinuity. Thus, even if a planar uniaxial state is unlikely to be caught numerically, its presence can be detected by the appearance of neat jumps in either the polar or azimuthal angles. In the limiting case where all three eigenvalues of $\mathbf{Q}_k$ are equal, they must necessarily vanish as $\mathbf{Q}_k$ is traceless; then the state is isotropic and $\boldsymbol{n}_k$ would accordingly degenerate in the whole unit sphere $\mathbb{S}^2$.

The order tensor $\mathbf{Q}_k$ defined in Eq. (7) differs by a factor $\frac{3}{2}$ from the order tensor more often employed in the literature on continuum theories [3]. In an alternative, equivalent representation, which also makes the link to tradition clearer, $\mathbf{Q}_k$ would read as

$$\mathbf{Q}_k = \frac{3}{2}S_k\left(\boldsymbol{n}_k \otimes \boldsymbol{n}_k - \frac{1}{3}\mathbf{I}\right) + \frac{3}{2}b_k(\boldsymbol{m}_k \otimes \boldsymbol{m}_k - \boldsymbol{\ell}_k \otimes \boldsymbol{\ell}_k), \tag{10}$$

where $(\boldsymbol{n}_k, \boldsymbol{m}_k, \boldsymbol{\ell}_k)$ is the eigenframe of $\mathbf{Q}_k$ and b_k and S_k must obey the inequalities

$$0 \leq b_k \leq \min\left\{S_k, \frac{1}{3}(1-S_k)\right\} \tag{11}$$

to confine Eq. (10) to represent all possible inequivalent states [52]. In this representation, a planar uniaxial state corresponds to the upper bound $b_k=S_k$ in (11). This bound together with the lower bound $b_k=0$ constitutes the whole variety of uniaxial states represented by Eq. (10); all other states are biaxial.

In the following section, we compute appropriate averages of the quantities θ_k, ϕ_k, S_k, and b_k across the cell, for different values of the cell's thickness d, of the reduced temperature T^*, and of the total twist angle Φ_0 between the anchoring orientations at the two substrates. These averages will describe equilibrium molecular textures within the cell, for which we are primarily interested in the corresponding torque distribution obtained from Eq. (4).

III. COMPUTATIONAL RESULTS

Equations (1) and (2) were discretized in time. After running over 200 000 time steps for equilibration, all character-

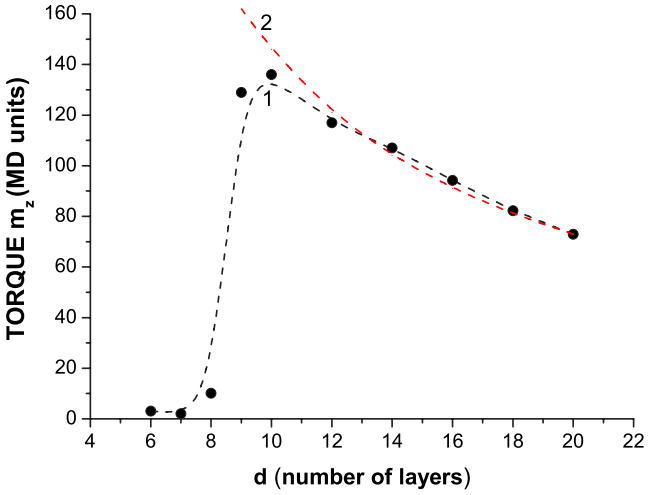

FIG. 1. (Color online) The torque m_z transmitted through the nematic twist cell against the cell's thickness d (measured in numbers of molecular layers): $T^*=0.55$, $V_{\text{LC-SB}}/V_{\text{LC-LC}}=10$, $\Phi_0=\frac{\pi}{2}$. Curve 1, results of MD simulations; curve 2, $\frac{1}{d}$ law.

istics of the system were also averaged over 200 000 time steps; averages obtained with larger numbers of time steps showed similar results. The set of averaged order parameters S_k and b_k, the averaged orientational angles θ_k and ϕ_k, and the averaged total forces and torques acting on the anchoring substrates were computed for several values of the cell's thickness d and of the reduced temperature T^*. The most significant of our computational results are illustrated by Figs. 1–7.

It was shown in [15] that the most meaningful measure of structural instability in the cell is the total torque transmitted from one substrate to the other at equilibrium. The lack of monotonicity in the torque's diagram against d was interpreted as the sign that a torque nanomachine can assess the

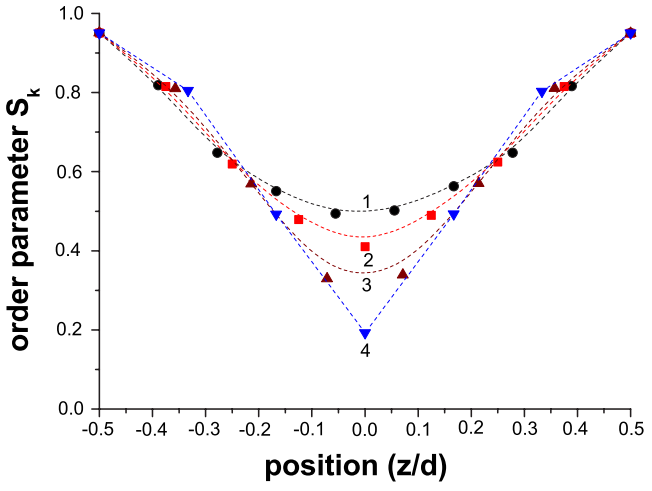

FIG. 2. (Color online) The orientational order parameter S_k across cells of different thickness d: $T^*=0.55$, $V_{\text{LC-SB}}/V_{\text{LC-LC}}=10$, $\Phi_0=\frac{\pi}{2}$. Curve 1, $d=10$; curve 2, $d=9$; curve 3, $d=8$; curve 4, $d=7$. All values of d are measured in numbers of molecular layers. Each graph is rescaled to the corresponding d, so that the domain of all graphs is $\left[-\frac{1}{2},\frac{1}{2}\right]$.

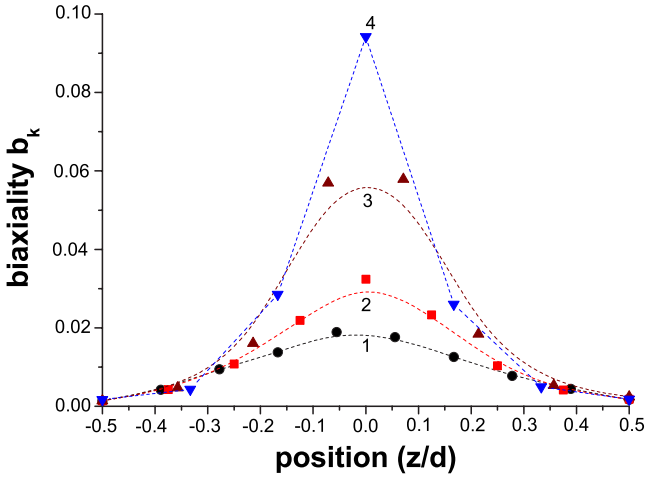

FIG. 3. (Color online) The biaxiality parameter b_k across cells of different thickness d: $T^*=0.55$, $V_{\text{LC-SB}}/V_{\text{LC-LC}}=10$, $\Phi_0=\frac{\pi}{2}$. Curve 1, $d=10$; curve 2, $d=9$; curve 3, $d=8$; curve 4, $d=7$. All values of d are measured in numbers of molecular layers. Each graph is rescaled to the corresponding d, so that the domain of all graphs is $\left[-\frac{1}{2},\frac{1}{2}\right]$.

textural change associated with a nematic order reconstruction inside the cell [15,16]. In Fig. 1, curve 1 shows the diagram of the z component m_z of the torque acting on one of the bounding substrates as a function of d obtained from our MD simulations for $T^*=0.55$ and total twist angle $\Phi_0=\frac{\pi}{2}$. While both the y and x components, m_y and m_x, of the same torque were found to be negligibly small relative to m_z ($m_y/m_z\simeq 10^{-2}$, $m_x/m_z\simeq 10^{-2}$), the corresponding components m_z', m_y', and m_x' of the torque acting on the opposite substrate were found to differ from m_z, m_y, and m_x essentially only in the sign ($m_z'/m_z\simeq -1.001$, $m_y'/m_y\simeq -1.02$, and $m_x'/m_x\simeq -0.97$). Here and in the following, d is measured in number of molecular layers. For comparison, in Fig. 1, curve

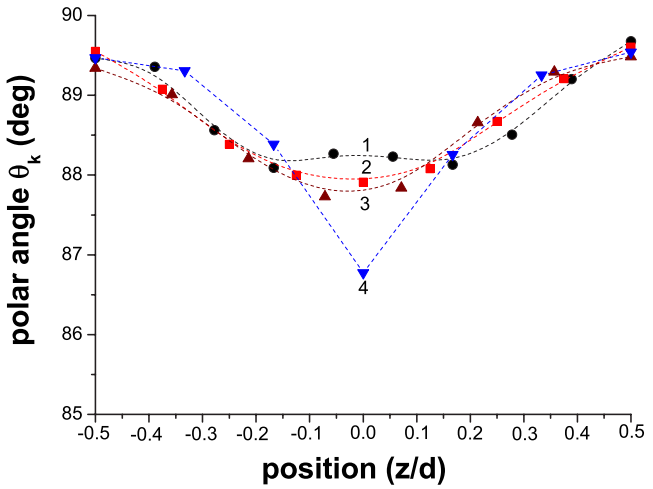

FIG. 4. (Color online) The polar angle θ_k across cells of different thickness d: $T^*=0.55$, $V_{\text{LC-SB}}/V_{\text{LC-LC}}=10$, $\Phi_0=\frac{\pi}{2}$. Curve 1, $d=8$; curve 2, $d=9$; curve 3, $d=8$; curve 4, $d=7$. All values of d are measured in numbers of molecular layers. Each graph is rescaled to the corresponding d, so that the domain of all graphs is $\left[-\frac{1}{2},\frac{1}{2}\right]$.

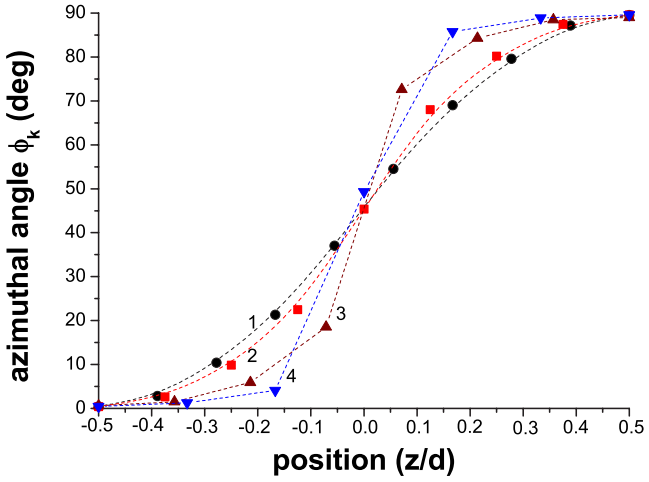

FIG. 5. (Color online) The azimuthal angle ϕ_k across cells of different thickness d: $T^*=0.55$, $V_{\text{LC-SB}}/V_{\text{LC-LC}}=10$, $\Phi_0=\frac{\pi}{2}$. Curve 1, $d=10$; curve 2, $d=9$; curve 3, $d=8$; curve 4, $d=7$. All values of d are measured in numbers of molecular layers. Each graph is rescaled to the corresponding d, so that the domain of all graphs is $[-\frac{1}{2},\frac{1}{2}]$.

2 shows the $\frac{1}{d}$ law predicted by the classical elastic theory [3]. It is easily seen that, for sufficiently thick cells ($d \geq 10$), the results of our MD simulations are very close to the classical law. However, when d is smaller than a critical value $d_c \simeq 10$, the diagram of the transmitted torque deviates significantly from the classical law. Instead of increasing as d decreases, m_z sharply decays down to nearly zero. This result is in good qualitative agreement with the behavior predicted in [15] by the continuum Landau theory.

To appreciate better the origin of such a decay, we show in Fig. 2 the profiles of the orientational order parameter S_k for cells of different thickness d. For either $d=10$ or $d=9$, S_k is sufficiently large throughout the cell. This means that the molecular texture is sufficiently ordered, and hence the

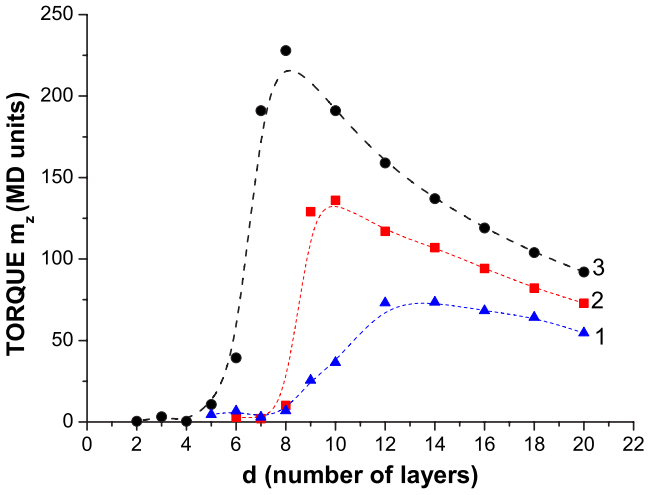

FIG. 6. (Color online) The torque m_z transmitted through the cell against the cell's thickness d (in numbers of molecular layers) for different reduced temperatures T^*: $V_{\text{LC-SB}}/V_{\text{LC-LC}}=10$, $\Phi_0=\frac{\pi}{2}$. Curve 1, $T^*=0.58$; curve 2, $T^*=0.55$; curve 3, $T^*=0.50$.

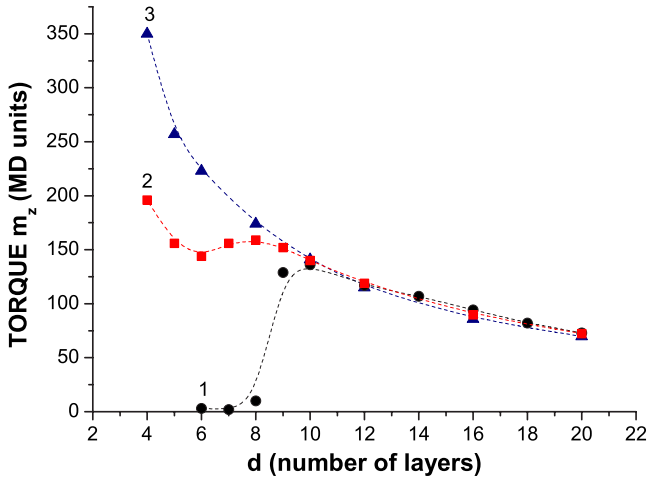

FIG. 7. (Color online) The torque m_z transmitted through the cell against the cell's thickness d (in numbers of molecular layers) for different values of the total twist angle Φ_0: $T^*=0.55$, $V_{\text{LC-SB}}/V_{\text{LC-LC}}=10$. Curve 1, $\Phi_0=\frac{\pi}{2}$; curve 2, $\Phi_0=0.47\pi$; curve 3, $\Phi_0=0.44\pi$.

torque induced by the torsion of one bounding substrate relative to the other can be successfully transmitted through the cell. On the other hand, when the cell's thickness is reduced to $d=8$ and $d=7$, S_k is appreciably smaller in the middle of the cell. Thus, thinner cells are more disordered.

This conclusion is also confirmed by Figs. 3–5, which show the biaxiality parameter b_k, the polar angle θ_k, and the azimuthal angle ϕ_k, respectively, across cells of different thickness. In the middle of the cell, the biaxiality parameter b_k increases as d decreases, approaching the upper limit $b_k=S_k$ for $d=7$. Correspondingly, the azimuthal angle ϕ_k exhibits a steeper increase, which for $d=7$ almost resembles a discontinuity. This suggests that a planar uniaxial state is about to develop in the (x,y) plane within the thinnest of the cells explored here ($d=7$), a conclusion consistent with the prediction of the continuum Landau theory extrapolated to the nanoscopic scale [15]. Figure 5 shows that for both $d=10$ and $d=9$ the azimuthal angle profile is nearly linear, as predicted by the classical elastic theory, whereas for both $d=8$ and $d=7$ the corresponding profile indicates two almost uniform molecular textures aligned in orthogonal directions (the total twist Φ_0 is here $\frac{\pi}{2}$), each close to one of the anchoring substrates, and both adjacent to an almost formed planar uniaxial state. The lack of order in sufficiently thin twist cells, associated with the gradual emergence of a planar uniaxial state, is eventually responsible for the lack of efficiency in the torque transmission from one substrate to the other, which results in the sharp decay in m_z when $d \leq d_c \simeq 10$.

In Fig. 6, m_z is plotted against d for different reduced temperatures ($T^*=0.58$, $T^*=0.55$, and $T^*=0.50$). It is easily seen that for sufficiently thick cells ($d \geq 10$), all graphs exhibit a growth of m_z with decreasing d until a certain maximum value $m_z^{(\max)}$ of the torque is reached. This growth is then followed by a decay in m_z as d is further decreased. In addition, the lower is T^*, the higher is $m_z^{(\max)}$, and the lower is the corresponding critical thickness d_c. These results can

be qualitatively understood as follows. When the temperature of the cell is close to the bulk nematic-to-isotropic transition point $T^*_{\mathrm{NI}}=0.61$, the orientational order in the sample is weakened, and the gradient of the nematic director field required to induce a high disorder in the cell should correspondingly be lower than that for a well developed nematic phase. Since, for a fixed value of the total twist angle Φ_0, the gradient of the nematic director field is inversely proportional to the cell's thickness d, the critical thickness d_c at which the decay in m_z occurs should decrease with decreasing temperature. As for the maximum value $m_z^{(\max)}$ of the torque transmitted through the cell, intuition suggests that at a lower temperature the orientational order in the cell is higher, and so the transmitted torque is accordingly larger.

Figure 7 shows the torques m_z as a function of d computed for three different values of the total twist angle Φ_0, namely, $\Phi_0=\frac{\pi}{2}$, $\Phi_0=0.47\pi$, and $\Phi_0=0.44\pi$, at fixed temperature $T^*=0.55$. For sufficiently thick cells ($d\geq 10$), all three graphs exhibit a growth in the torque m_z with decreasing d, which is very close to the classical $\frac{1}{d}$ law. However, for smaller values of d, Fig. 7 illuminates three different behaviors, depending on the value of Φ_0. For $\Phi_0=\frac{\pi}{2}$, m_z decays sharply to nearly zero as d is decreased below $d_c\simeq 10$. For $\Phi_0=0.47\pi$, m_z reaches a maximum value at $d\simeq 8$ and then decays to a positive minimum at $d\simeq 6$, to eventually grow again upon further decreasing d. Finally, for $\Phi_0=0.44\pi$, m_z exhibits a steady, monotonic growth as d decreases. These simulation results are in rather good agreement with the predictions of [15]: there is a critical value of the total twist angle $\Phi_0^{(c)}$, below which the classical elastic theory can be extrapolated down to the nanoscopic scale; for $\Phi_0>\Phi_0^{(c)}$, however, a molecular order reconstruction, foreign to the classical theory, takes place in the twist cell, which has one of its most appreciable consequences in the behavior of the transmitted torque.

It is instructive to compare the absolute values of the torque m_z obtained from our MD simulations with the values predicted in [15]. According to Fig. 6, for $\Phi_0=\frac{\pi}{2}$ and $T^*=0.50$, $m_z^{(\max)}\simeq 230$ MD units. The MD unit of torque is the same as the MD unit of energy [47], i.e., $V_{\text{LC-LC}}$. For $T^*=k_BT/V_{\text{LC-LC}}=0.5$, $V_{\text{LC-LC}}=2k_BT$, and so taking $T\simeq 300$ K as the typical temperature of a nematic phase, we easily obtain $V_{\text{LC-LC}}\simeq 8.3\times 10^{-14}$ erg. Therefore, we estimate $m_z^{(\max)}\simeq 1.9\times 10^{-11}$ erg. In our MD simulations, the simulation box is $22r_0\times 22r_0\times 22r_0$ in size, and the substrate surface is $20r_0\times 20r_0$, where r_0 is of the order of a molecular length, i.e., $r_0\simeq 2.5\times 10^{-7}$ cm. Thus, the actual substrate area is about 2.5×10^{-11} cm^2, and correspondingly the maximum value of the torque per unit area is about 0.76 erg cm^{-2}. We derive from Fig. 2 in [15] that for the same maximum torque density the continuum Landau theory predicts a value of approximately 1.5 erg cm^{-2}, which agrees with our molecular estimate.

Finally, a general remark should also be made about the accuracy of our computations. It is well known (see, for example, [53]) that $1/\sqrt{N}$ is a measure of the relative uncertainty $\delta f/f$, where f is an average value of the observable f and δf is a mean square fluctuation for the same observable. Accordingly, since each layer in the confined LC cell studied above contains 338 spins, the relative uncertainty for all computed observables does not exceed 6%.

IV. CONCLUSION

We studied with the methods of molecular dynamics the equilibrium molecular textures within a nematic twist cell. We showed that for sufficiently thick cells the average molecular profile agrees with the linear twist law predicted by the classical elastic theory. However, upon decreasing the cell's thickness d below a critical value d_c, estimated close to ten molecular lengths, the equilibrium molecular textures change dramatically: a planar uniaxial state develops between two nearly uniform alignments imposed by the anchoring substrates, and correspondingly the torque transmitted from one bounding plate to the other is not monotonic as a function of d, provided the total twist angle exceeds a critical value. Thus, at the plates' separation where the transmitted torque exhibits its local maximum, an ideal torque nanomachine should suffer a snapping instability as the torque is further increased.

These conclusions follow rather closely the predictions of the continuum Landau theory applied to a nanoconfined twist cell [15]. All of our computations were in MD units. To achieve a quantitative comparison between continuum and molecular methods, we also converted in absolute units the torque per unit surface area corresponding to the onset of the snapping instability: we found a value approximately one-half of the one predicted in [15]. On account of the approximations involved in the MD simulations, such as the lack of anisotropy in the molecular inertia and the peculiar model pair potential, this should be regarded as a fairly good quantitative agreement.

We believe that this agreement constitutes a proof of principle that a continuum Landau theory can safely be applied to nanoconfined liquid crystals, at least as long as its predictions concern appropriate global mechanical quantities; we are aware that other phenomena such as surface-induced layers, density modulations, orientational pretilts, and similar fine details of the molecular organization (see, for example, [21–23,28,35,36]) cannot possibly be captured by a Landau theory. Accordingly, with similar provisos, this result also encourages us to extrapolate to the nanoscopic scale continuum Landau theories appropriate for other soft matter systems.

ACKNOWLEDGMENTS

This work was in part carried out at the Dipartimento di Matematica, Università di Pavia, Italy, where L.V.M. was visiting and was supported by the Cariplo Foundation through the Landau Network, Centro Volta (Como, Italy); both financial support and scientific hospitality are gratefully acknowledged.

[1] Ph. Martinot-Lagarde, H. Dreyfus-Lambez, and I. Dozov, Phys. Rev. E **67**, 051710 (2003).
[2] L. Komitov, G. Hauck, and H. D. Koswig, Phys. Status Solidi A **97**, 645 (1986).
[3] P. G. de Gennes and J. Prost, *The Physics of Liquid Crystals* (Oxford University Press, Oxford, 1993).
[4] R. Barberi, F. Ciuchi, G. E. Durand, M. Iovane, D. Sikharulidze, A. M. Sonnet, and E. G. Virga, Eur. Phys. J. E **13**, 61 (2004).
[5] R. Barberi, F. Ciuchi, G. Lombardo, R. Bartolino, and G. E. Durand, Phys. Rev. Lett. **93**, 137801 (2004).
[6] S. Joly, I. Dozov, and Ph. Martinot-Lagarde, Phys. Rev. Lett. **96**, 019801 (2006).
[7] R. Barberi, F. Ciuchi, H. Ayeb, G. Lombardo, R. Bartolino, and G. E. Durand, Phys. Rev. Lett. **96**, 019802 (2006).
[8] I. Dozov, M. Nobili, and G. Durand, Appl. Phys. Lett. **70**, 1179 (1997).
[9] H. Ayeb, F. Ciuchi, G. Lombardo, R. Barberi, and G. E. Durand (unpublished).
[10] S. Kralj, E. G. Virga, and S. Žumer, Phys. Rev. E **60**, 1858 (1999).
[11] N. Schopohl and T. J. Sluckin, Phys. Rev. Lett. **59**, 2582 (1987).
[12] M. Ambrožic, S. Kralj, and E. G. Virga, Phys. Rev. E **75**, 031708 (2007).
[13] Y. Zhang, B. Wang, D. B. Chung, J. Colegrove, and P. J. Bos, SID Intl. Symp. Digest Tech. Papers **36**, 1782 (2005).
[14] F. Bisi, E. C. Gartland, Jr., R. Rosso, and E. G. Virga, Phys. Rev. E **68**, 021707 (2003).
[15] F. Bisi, E. G. Virga, and G. E. Durand, Phys. Rev. E **70**, 042701 (2004).
[16] F. Bisi and E. G. Virga, in *Modeling of Soft Matter*, edited by M.-C. T. Calderer and E. M. Terentjev (Springer, New York, 2005), pp. 111–132.
[17] B. Zappone, Ph. Richetti, R. Barberi, R. Bartolino, and H. T. Nguyen, Phys. Rev. E **71**, 041703 (2005).
[18] G. McKay and E. G. Virga, Phys. Rev. E **71**, 041702 (2005).
[19] M. M. Telo da Gama, Physica A **244**, 389 (1999).
[20] M. K. Chalam, K. E. Gubbins, E. de Miguel, and L. F. Rull, Mol. Phys. **7**, 357 (1991).
[21] Z. Zhang, A. Chakrabarti, O. G. Mouritsen, and M. J. Zuckermann, Phys. Rev. E **53**, 2461 (1996).
[22] G. D. Wall and D. J. Cleaver, Phys. Rev. E **56**, 4306 (1997).
[23] T. Gruhn and M. Schoen, Phys. Rev. E **55**, 2861 (1997).
[24] T. Gruhn and M. Schoen, J. Chem. Phys. **108**, 9124 (1998).
[25] P. Pasini, C. Chiccoli, and C. Zannoni, in *Advances in the Computer Simulations of Liquid Crystals*, edited by P. Pasini and C. Zannoni (Kluwer, Dordrecht, 2000), pp. 121–137.
[26] C. Chiccoli, S. Guzzetti, P. Pasini, and C. Zannoni, Mol. Cryst. Liq. Cryst. **360**, 119 (2001).
[27] M. Dijkstra, R. van Roij, and R. Evans, Phys. Rev. E **63**, 051703 (2001).
[28] D. J. Cleaver and P. I. C. Teixeira, Chem. Phys. Lett. **338**, 1 (2001).
[29] J. Quintana, E. C. Poiré, H. Domínguez, and J. Alejandre, Mol. Phys. **100**, 2597 (2002).
[30] K. Venu, V. S. S. Sastry, and K. P. N. Murthy, Europhys. Lett. **58**, 646 (2002).
[31] N. V. Priezjev, G. Skačej, R. A. Pelcovits, and S. Žumer, Phys. Rev. E **68**, 041709 (2003).
[32] S. Kondrat, A. Poniewierski, and L. Harnau, Europhys. Lett. **10**, 163 (2003).
[33] R. Memmer and O. Fliegans, Phys. Chem. Chem. Phys. **5**, 558 (2003).
[34] C. Chiccoli, P. Pasini, A. Šarlah, C. Zannoni, and S. Žumer, Phys. Rev. E **67**, 050703(R) (2003).
[35] H. Steuer, S. Hess, and M. Schoen, Phys. Rev. E **69**, 031708 (2004).
[36] D. Micheletti, L. Muccioli, R. Berardi, M. Ricci, and C. Zannoni, J. Chem. Phys. **123**, 224705 (2005).
[37] A. Poniewierski and R. Hołyst, Phys. Rev. A **38**, 3721 (1988).
[38] A. M. Somoza, L. Mederos, and D. E. Sullivan, Phys. Rev. E **52**, 5017 (1995).
[39] T. J. Sluckin, Physica A **213**, 105 (1995).
[40] M. M. Telo da Gama, Physica A **172**, 219 (1991).
[41] I. Rodríguez-Ponce, J. M. Romero-Enrique, E. Velasco, L. Mederos, and L. F. Rull, Phys. Rev. Lett. **82**, 2697 (1999).
[42] A. N. Shalaginov and D. E. Sullivan, Phys. Rev. E **63**, 031704 (2001).
[43] I. Rodríguez-Ponce, J. M. Romero-Enrique, and L. F. Rull, Phys. Rev. E **64**, 051704 (2001).
[44] M. P. Allen, Mol. Phys. **96**, 1391 (1999).
[45] A. Chrzanowska, P. I. C. Teixeira, H. Ehrentraut, and D. J. Cleaver, J. Phys.: Condens. Matter **13**, 4715 (2001).
[46] D. Andrienko and M. P. Allen, Phys. Rev. E **65**, 021704 (2002).
[47] M. P. Allen and D. J. Tildesly, *Computer Simulations of Liquids* (Clarendon, Oxford, 1989).
[48] W. L. McMillan, Phys. Rev. A **4**, 1238 (1971).
[49] W. Maier and A. Saupe, Z. Naturforsch. A **13A**, 564 (1958); T. J. Sluckin, D. Dunmur, and H. Stegemeyer, *Crystals that Flow* (Taylor and Francis, London, 2004), pp. 381–385, English translation.
[50] *Defects in Liquid Crystals: Computer Simulations, Theory and Experiments*, edited by O. D. Lavrentovich, P. Pasini, C. Zannoni, and S. Žumer (Kluwer, Dordrecht, 2001).
[51] C. Zannoni, in *The Molecular Physics of Liquid Crystals*, edited by G. R. Luckhurst and G. W. Gray (Academic, New York, 1979), pp. 51–83.
[52] G. De Matteis, S. Romano, and E. G. Virga, Phys. Rev. E **72**, 041706 (2005).
[53] L. D. Landau and E. M. Lifshits, *Statistical Physics*, 3rd ed. (Nauka, Moscow, 1976), Part 1.